JBC RESEARCH ARTICLE

Depletion of plasma thymidine results in growth retardation and mitochondrial myopathy in mice overexpressing human thymidine phosphorylase

Received for publication, June 16, 2022, and in revised form, February 6, 2023 Published, Papers in Press, February 10, 2023,
https://doi.org/10.1016/j.jbc.2023.103002

Naomoto Harada*, Haruka Nagasaki, Hiromi Yamamoto, Kenji Matsubara, Takamasa Suzuki, Akira Gomori, Tatsushi Yokogawa, Kenichi Matsuo, and Kazutaka Miyadera

From the Discovery and Preclinical Research Division, Taiho Pharmaceutical Co Ltd, Tsukuba, Ibaraki, Japan

Reviewed by members of the JBC Editorial Board. Edited by Craig Cameron

Plasma thymidine levels in rodents are higher than in other mammals including humans, possibly due to a different pattern and lower level of thymidine phosphorylase expression. Here, we generated a novel knock-in (KI) mouse line with high systemic expression of human thymidine phosphorylase to investigate this difference in nucleotide metabolism in rodents. The KI mice showed growth retardation around weaning and died by 4 weeks of age with a decrease in plasma thymidine level compared with the litter-control WT mice. These phenotypes were completely or partially rescued by administration of the thymidine phosphorylase inhibitor 5-chloro-6-(2-iminopyrrolidin-1-yl) methyl-2,4(1H,3H)-pyrimidinedione hydrochloride or thymidine, respectively. Interestingly, when thymidine phosphorylase inhibitor administration was discontinued in adult animals, KI mice showed deteriorated grip strength and locomotor activity, decreased bodyweight, and subsequent hind-limb paralysis. Upon histological analyses, we observed axonal degeneration in the spinal cord, muscular atrophy with morphologically abnormal mitochondria in quadriceps, retinal degeneration, and abnormality in the exocrine pancreas. Moreover, we detected mitochondrial DNA depletion in multiple tissues of KI mice. These results indicate that the KI mouse represents a new animal model for mitochondrial diseases and should be applicable for the study of differences in nucleotide metabolism between humans and mice.

Nucleosides play important roles as precursors to nucleotides needed for DNA and RNA biosynthesis (1). The metabolism of thymidine, a pyrimidine deoxynucleoside, is regulated by two enzymes, thymidine phosphorylase (TP) and thymidine kinase (TK). TP catalyzes the phosphorolysis of thymidine to thymine and 2′-deoxyribose 1-phosphate, whereas TK phosphorylates thymidine to dTMP, and both play important roles in nucleotide salvage and homeostasis (2, 3).

Mutations in the human TP gene (*TYMP*) cause mitochondrial neurogastrointestinal encephalopathy (MNGIE), an autosomal-recessive disease characterized by ptosis, progressive external ophthalmoparesis, gastrointestinal dysmotility, cachexia, peripheral neuropathy, and leukoencephalopathy (4). In patients with MNGIE with *TYPM* mutations, plasma thymidine levels are increased more than 20-fold compared with healthy controls, which probably causes a mitochondrial nucleotide pool imbalance, leading to mtDNA alterations, *via* a mitochondria-specific thymidine salvage pathway (5). However, in mice, TP is mainly expressed in the liver and intestine, whereas uridine phosphorylase (UP), which also shows a weak substrate specificity for thymidine, is predominantly expressed in other tissues (6–8); meanwhile, TP is expressed in multiple tissues throughout the human body (Fig. 1). As a result, the plasma level of thymidine in mice is about 10-fold higher than in humans (9). Therefore, although the plasma thymidine level was elevated in *Tymp* KO (TP-KO) and *Tymp/Upp1* double KO (TP/UP-dKO) mice, it was only two or five times that of the WT mice, respectively (10). Consequently, none of the TP-KO, UP-KO (*Upp1* KO), and TP/UP-dKO mice showed major symptoms of MNGIE, while leukoencephalopathy was observed only in aged TP/UP-dKO mice (10–12).

On the other hand, mutations in the human mitochondrial TK gene (*TK2*) cause mtDNA depletion syndrome (MDS), an autosomal-recessive disease characterized by a reduction in mtDNA copy number in affected tissues, which leads to progressive myopathy, hepatopathy, or encephalopathy (13). Unlike TP/UP-dKO mice, *Tk2*-deficient (knockout or H126N-mutation KI) mice show depletion of the mitochondrial deoxythymidine triphosphate (dTTP) pool and DNA copy number in various tissues and die within 2 to 4 weeks of birth with development of neurodegeneration and muscle atrophy, which are some of the symptoms observed in human MDS (14–16). Therefore, the Tk2-deficient mouse model appears to mimic human MDS.

We hypothesize that one of the reasons why TP-KO and TP/UP-DKO mice do not recapitulate most of the human MNGIE phenotypes might be their higher plasma thymidine level compared with humans. To explore this possibility, we generated a novel transgenic mouse strain that overexpresses human TP systemically and succeeded in reducing plasma thymidine levels to almost the same level as in humans.

* For correspondence: Naomoto Harada, nm-harada@taiho.co.jp.

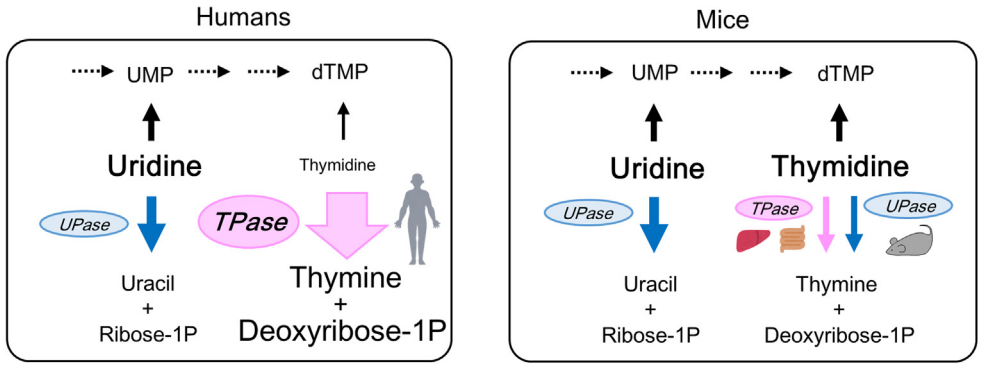

Figure 1. Thymidine metabolism in humans and mice. Schematic representation of thymidine metabolism in humans and mice. In humans, thymidine phosphorylase (TPase) is expressed in multiple tissues throughout the body. In mice, TPase is mainly expressed in the liver and intestine, whereas uridine phosphorylase (UPase), which also shows weak substrate specificity for thymidine, is predominantly expressed in other tissues throughout the body. As a result, the plasma thymidine level in mice is higher than that in humans.

Here, we report the phenotype of R26-hTP-KI mice during the growth period, as well as in the postmaturation period by regulating *in vivo* TP activity with TPI administration.

Results

Generation of human TP KI mice

In mice, TP is predominantly expressed in the liver and intestine, while UP, which also shows weak substrate specificity for thymidine, is expressed in other tissues (7). Therefore, we first generated Upp1-hTP-KI mice, in which the human TP gene (*TYMP*) was knocked-into the mouse UP gene (*Upp1*) locus (Fig. 2*A*). As expected, expression of human *TP* mRNA was detected in various tissues such as thymus, heart, lung, spleen, kidney, stomach, intestine, and brain where mouse *Upp1* mRNA was expressed, while mouse *Tymp* mRNA was predominantly expressed in the liver, intestine, and lung (Fig. 2*B*). Although TP activity in the intestine of Upp1-hTP-KI mice was increased compared with that in WT mice, total thymidine degrading activity (*i.e.*, sum of TP and UP activity) was not changed, since UP activity in the KI mice was lower than that in WT mice (Fig. 2*C*). As a result, plasma thymidine levels in KI mice were not changed compared with WT mice (Fig. 2*D*). These results suggested that expression of the human TP gene from the mouse *Upp1* allele was not sufficient to decrease plasma thymidine levels and higher expression of the TP gene was required.

Next, in order to improve the TP gene expression, we constructed a targeting vector to integrate a human TP gene expression cassette (CMV-hTP-pA) into the mouse *Gtrosa26* locus (17), as shown in Figure 3*A*. After electroporation of the targeting vector into mouse ES cells, homologous recombinant ES clones were obtained, confirmed by Southern blot analysis (Fig. 3*B*), and then injected into C57BL/6N blastocysts. Germline-transmitted chimeras were crossbred with C57BL/6N females, and heterozygous offspring (*Gtrosa26*$^{tm3\ (CMV\text{-}hTP)Tai}$) were born and designated as R26-hTP KI mice.

Heterozygous R26-hTP-KI mice were normal and healthy at birth and did not differ in bodyweight from that of the litter-control WT mice. However, after 14 days, the KI mice showed growth retardation with significantly lower bodyweight compared with the WT animals (Fig. 3*C*), and they subsequently showed hind-limb paralysis and were euthanized at 4 weeks of age (Fig. 3*D*). Plasma thymidine was at an undetectable level (lower than 10 nM) in 21-day-old KI mice and 1.51 ± 0.48 μM in the litter-control WT mice (Fig. 3*E*).

TP protein expression and thymidine degrading activity in R26-hTP-KI mice

To examine whether human TP protein was expressed systemically in R26-hTP-KI mice, tissue lysates were prepared from the brain, thymus, heart, lung, liver, stomach, intestine, pancreas, spleen, and kidney of R26-hTP-KI and litter-control WT mice at 21 days of age and subjected to Western blot analysis. As shown in Figure 4*A*, human TP protein was expressed in all tissues examined in the R26-hTP-KI mice but not in the WT mice. Consistent with the protein expression profile, thymidine degrading activity in these tissues of R26-hTP-KI mice ranged from 140 ± 13 to 710 ± 170 nmol/h/mg, which was much higher than that in WT mice, where 54 ± 17 nmol/h/mg in the liver was the highest activity (Fig. 4*B*). These results suggested that the human TP protein expressed in the R26-hTP-KI mice degraded thymidine systemically, which resulted in decreased plasma thymidine levels.

Effect of TPI and thymidine on bodyweight loss in R26-hTP-KI mice

To confirm that the growth retardation and lethal phenotype in R26-hTP-KI mice were caused by the overexpression of the human TP gene, we administered a TPI (6) *i.p.* to the 2-week-old R26-hTP-KI mice every 2 or 3 days. As shown in Figure 5*A*, the bodyweight of R26-hTP-KI mice administered 100 mg/kg of TPI, but not those administered vehicle, increased almost the same as the litter-control WT mice. Furthermore, administration of 100 mg/kg of thymidine to R26-hTP-KI mice rescued their lethal phenotype, although the effect on bodyweight loss was partial compared with that of TPI administration (Fig. 5*B*). By continuous administration of TPI (50 mg/kg, twice a week), both male and female R26-hTP-KI mice survived more than half a year, although the

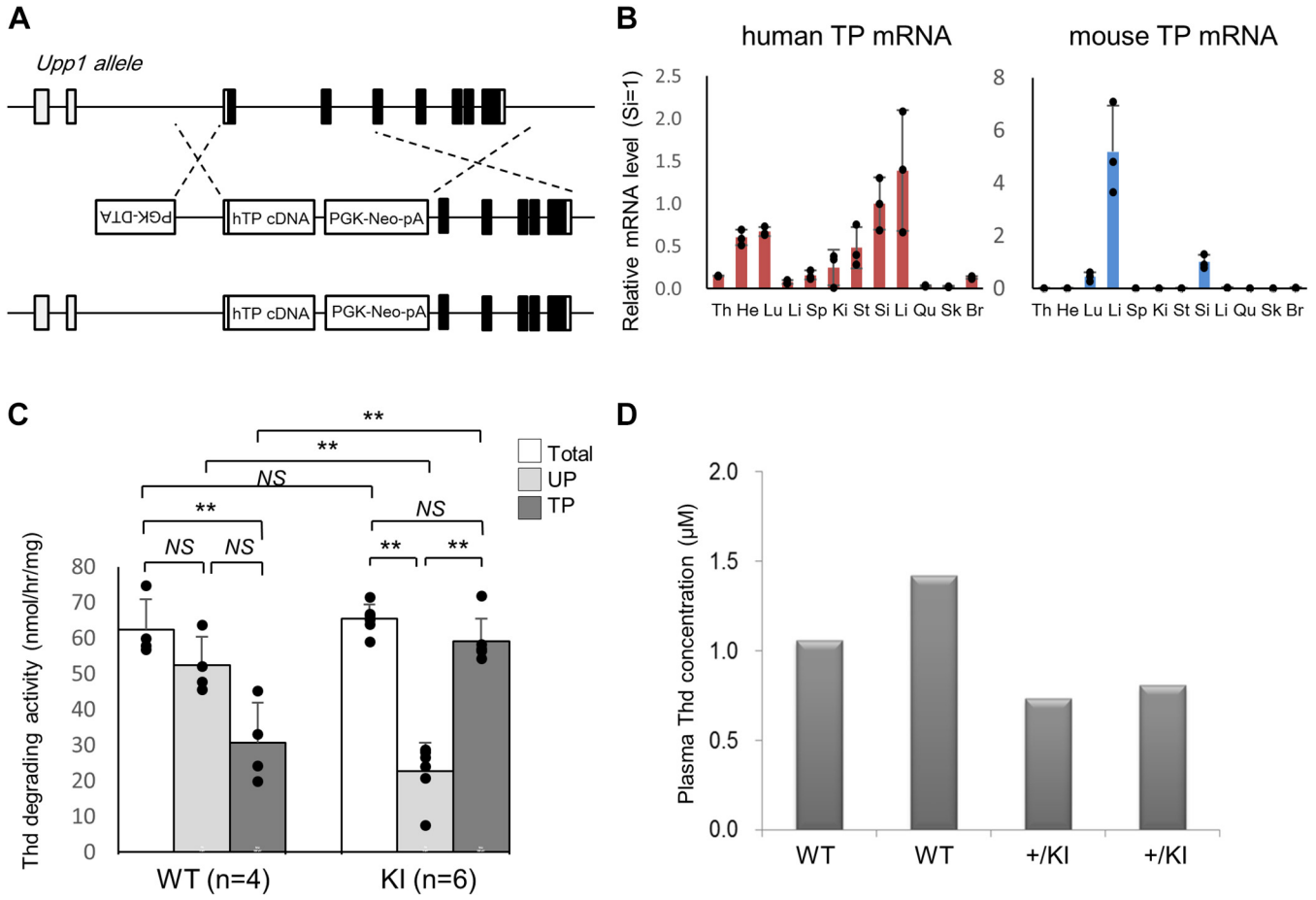

Figure 2. Analysis of Upp1-hTP-KI mice. *A*, schematic representation of the murine Upp1 locus (*top*), the targeting vector (*middle*), and the targeted allele (*bottom*). Coding and noncoding regions in exons are shown as hatched and open boxes, respectively. The PGK-DTA, hTP-cDNA, and PGK-neo-pA cassettes are shown as open boxes. *B*, human (*left*) and mouse (*right*) TP mRNA levels in Upp1-hTP-KI mouse tissues. Results are shown relative to the expression level in the small intestine. *C*, Thd degrading activities in the liver of WT (n = 4) and heterozygous KI (n = 6) mice. Total, UP, and TP activity are shown as *open*, *gray*, and *hatched bars*, respectively. $^{**}p < 0.01$. *D*, plasma Thd concentration in WT (n = 2) and heterozygous KI (n = 2) mice.

bodyweight of R26-hTP-KI mice was slightly lower than that of the litter-control WT mice (Fig. 6, *A* and *B*). The reproduction rate of female heterozygous R26-hTP KI mice was extremely low in both the backcross to male C57BL/6 mice and the intercross with male heterozygous R26-hTP-KI mice, and homozygous R26-hTP-KI mice were seldom born (data not shown). Therefore, heterozygous R26-hTP-KI mice were backcrossed to female C57BL/6 mice, and the obtained heterozygous R26-hTP-KI mice were used in all experiments in this study.

Next, we explored the impact of TPI administration on the plasma thymidine level in R26-hTP KI mice. Plasma thymidine level was rapidly increased and reached the maximum level (1.76 ± 0.52 μM) at 1 h after 50 mg/kg of TPI administration, then gradually decreased to the detection limit level (0.03 ± 0.02 μM) within 24 h of administration (Fig. 7). A similar pattern of plasma thymidine level was observed in control WT mice after TPI treatment, but plasma thymidine concentrations in WT mice were always higher than those in heterozygous KI mice (Fig. 7). There was no significant difference in plasma uridine/cytidine level between WT and heterozygous KI mice, and they were not affected by TPI administration. Plasma adenosine/guanosine level was under the detection limit and did not change after TPI administration (Table 1).

Effect of TPI-treatment discontinuation on R26-hTP-KI mice

To examine the importance of high plasma thymidine levels in adult mice, we discontinued the TPI-rescue in 7-month-old R26-hTP-KI mice. The bodyweight of R26-hTP-KI mice did not change until the second week, but it started to decrease rapidly during the third week (Fig. 8*A*). Concomitantly, the animals showed hind-limb paralysis (Fig. 8*B*) and decreases in both locomotor activity and grip strength (Fig. 8, *C* and *D*). Notably, locomotor activity and grip strength of R26-hTP-KI mice started to decrease around day 10, while bodyweight loss was observed after day 14. None of the decreases in bodyweight, locomotor activity, and grip strength as well as hind-limb paralysis were observed in the litter-control WT mice (Fig. 8, *A*–*D*). These results indicated that plasma thymidine levels were essential not only for normal growth during development but also for a normal physiological state in adult mice.

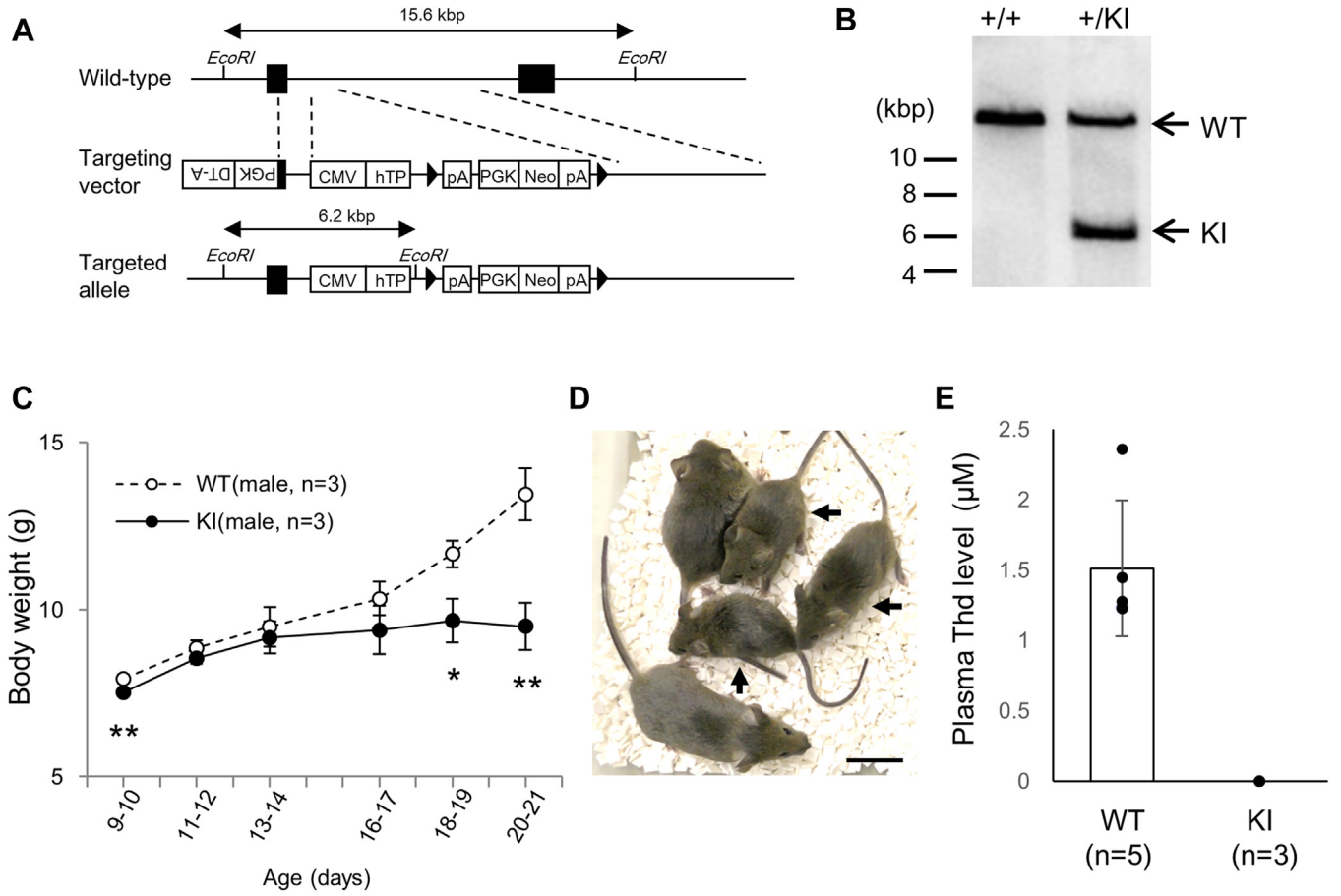

Figure 3. Generation of R26-hTP KI mice. *A*, schematic representation of the murine *Gtrosa26* locus (*top*), the targeting vector (*middle*), and the targeted allele (*bottom*). Exons are shown as *black boxes*, whereas the PGK-DTA, CMV-hTP, polyA, and PGK-neo-pA cassettes are shown as *open boxes*. The loxP sequences are shown as *black triangles*. The 15.6- and 6.2-kbp EcoRI fragments detected by Southern hybridization are shown. *B*, Southern blot analysis of WT (+/+) and heterozygous (+/KI) mice. *Arrows* indicate WT (15.6 kbp) and targeted (KI; 6.2 kbp) alleles. The position of size markers is shown on the *left*. *C*, bodyweight of WT (*open circle*, n = 3) and heterozygous KI (*closed circle*, n = 3) mice. Results are shown as means ± SD. $^{**}p < 0.01$ and $^{*}p < 0.05$ compared with the WT mice. *D*, photograph of littermate pups. The *arrows* indicate heterozygous KI mice. The scale bar represents 2 cm. *E*, plasma thymidine concentration in WT (n = 5) and heterozygous KI (n = 3) mice. Results are shown as means ± SD. The plasma thymidine level was undetectable in the KI mice.

Muscle atrophy and neural degeneration in R26-hTP-KI mice

To obtain further insight into the pathological features observed in R26-hTP-KI mice, various tissues (whole brain, eye, thymus, heart, lung, liver, stomach, intestine, pancreas, spleen, kidney, spinal cord, sciatic nerve, quadriceps, etc.) were prepared from the R26-hTP-KI mice showing hind-limb paralysis as adults and growth retardation around the weaning period, as well as their age-matched WT mice, and were subjected to histological examination (Fig. 9). As described below, abnormal findings were mainly observed in the quadriceps, spinal cord, sciatic nerve, and eye of R26-hTP-KI mice, but not in any tissues of WT mice. In the quadriceps of R26-hTP-KI mice, necrosis and degeneration of muscle fibers with partial hyalinization or nonuniformly striped hematoxylin and eosin (H&E) staining pattern were observed. In addition, regeneration of muscle cells and infiltration of inflammatory cells were observed (Fig. 9, *A* and *B*). Upon ultrastructural examination with electron microscopy (EM), sarcomeres showed abnormal morphology and giant mitochondria were accumulated beneath the fascia of R26-hTP-KI mice (Fig. 10, *A*–*D*), and some of them contained linearized high-electron-density cristae (18). In the ventral root of the spinal nerve of WT mice, fine lace-like structures of the myelin sheath were observed, while atrophic (eosinophilic) axon and myelin and reactive cells were increased in R26-hTP-KI mice (Fig. 9, *D* and *E*). Upon EM, uniformly sized myelinated axons were regularly arranged in WT mice. However, axonal degenerations (thinning of the myelin sheath, demyelination, and vacuole-like structures with low electron density) were predominantly observed in the ventral root of R26-hTP-KI mice. Some of the axons in R26-hTP-KI mice were surrounded by Schwann cells and seemed to be regenerating (Fig. 10, *E* and *F*). These findings, except for demyelination, were also observed in the sciatic nerve of the R26-hTP-KI mice (Figs. 9, *G* and *H* and 10, *G* and *H*). Notably, in the eye of R26-hTP-KI mice, thinning of the outer nuclear layer and rod and cone layers was observed in the retina (Fig. 9, *J* and *K*). In the exocrine pancreas of R26-hTP-KI mice, increased eosinophilic and decreased basophilic regions were observed with H&E, indicating zymogen granules

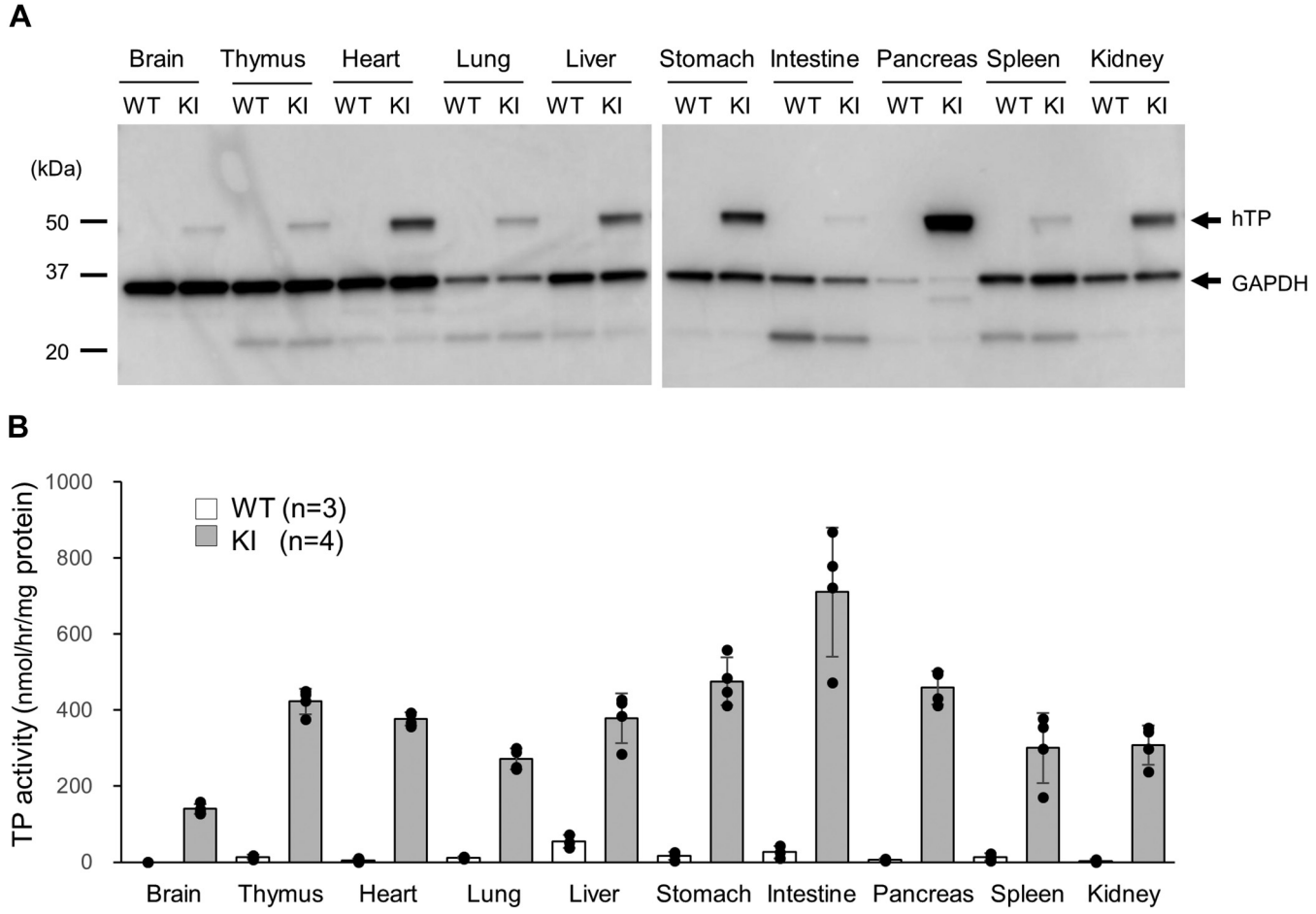

Figure 4. Systemic expression of human TP in R26-hTP-KI mice. *A*, Western blot analysis of human TP protein in the brain, thymus, heart, lung, liver, stomach, intestine, pancreas, spleen, and kidney of WT and KI mice. Total protein was loaded onto a gradient (4–15%) polyacrylamide gel electrophoresis gel (50 μg/lane) and detected with anti-human TP (1:200) and anti-GAPDH (1:1000) antibodies. *B*, TP activities in the brain, thymus, heart, lung, liver, stomach, intestine, pancreas, spleen, and kidney of WT (*open bars*, n = 3) and heterozygous KI (*closed bars*, n = 4) mice. Results are shown as means ± SD.

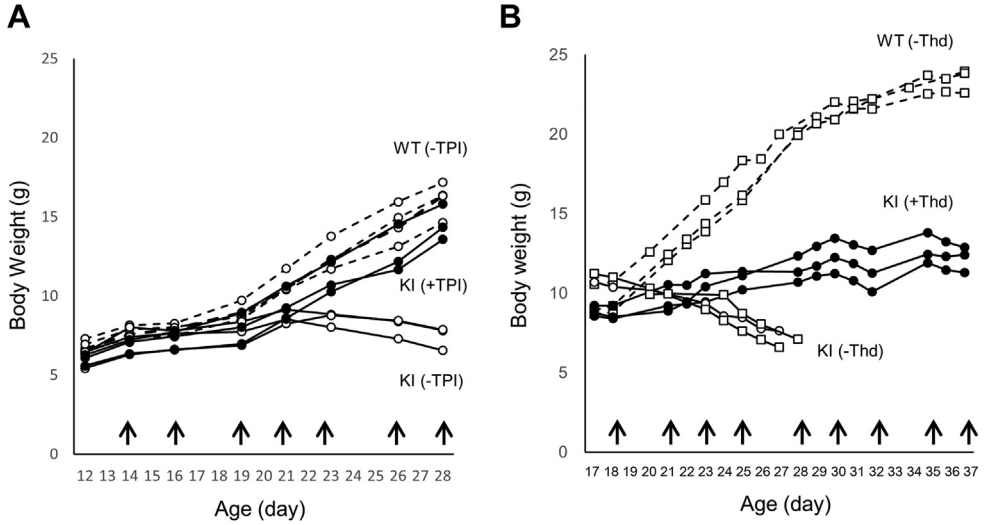

Figure 5. Effects of TPI and thymidine on bodyweight. *A*, bodyweight of WT and heterozygous KI mice with (*closed symbols*) or without (*open symbols*) TPI treatment. The *circles* and *squares* indicate female and male mice, whereas *dotted* and *solid lines* indicate WT and heterozygous KI mice, respectively. *Arrows* show the schedule of TPI treatment. *B*, bodyweight of WT and heterozygous KI mice with (*closed symbols*) or without (*open symbols*) thymidine treatment. *Arrows* show the schedule of thymidine treatment. TPI, thymidine phosphorylase inhibitor.

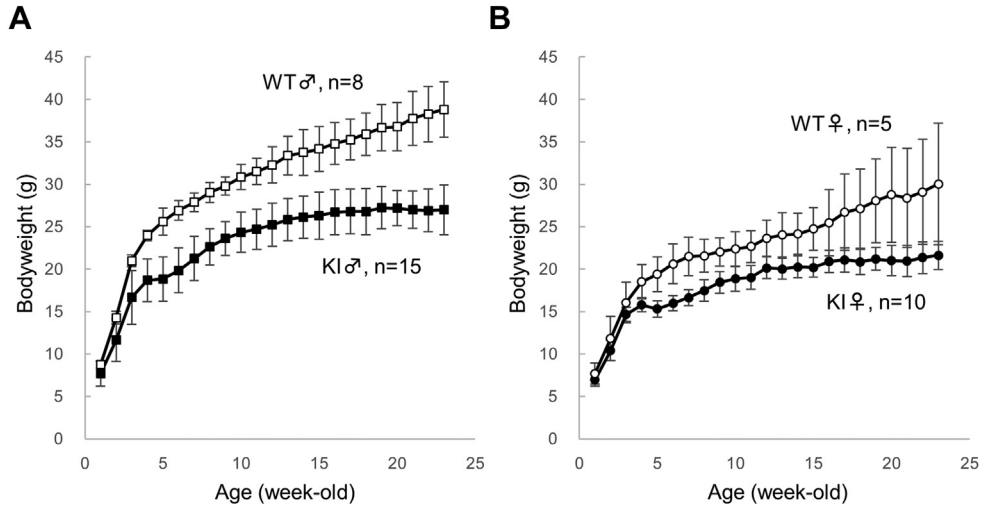

Figure 6. Long-term administration of TPI to T26-hTP-KI mice. *A*, bodyweight of male WT (*open squares*, n = 8) and KI (*closed squares*, n = 15) mice. *B*, bodyweight of female WT (*open circles*, n = 5) and KI mice (*closed circles*, n = 10). Data are shown as means ± SD.

should be increased (Fig. 9, *M* and *N*). No abnormal phenotype was observed in other tissues of R26-hTP-KI mice, except for degeneration/regeneration of tubules and urinary casts in the kidney (data not shown). Basically, similar pathological features were observed in the juvenile (around the weaning period) R26-hTP-KI mice without TPI treatment (Fig. 9, *C*, *F*, *I*, and *L*). These observations indicate that depletion of plasma thymidine in mice caused neurodegeneration and muscle atrophy with morphologically abnormal mitochondria, which are often found in human mitochondrial myopathies (18).

Decrease of mtDNA copy number in R26-hTP-KI mice

Decreases of mtDNA copy number have been reported in various types of human diseases including mitochondrial myopathies (19). Therefore, using quantitative real-time PCR, we measured mtDNA copy number in various tissues of the R26-hTP-KI mice showing symptoms of mitochondrial myopathies. In all tissues prepared from the R26-hTP-KI mice around the weaning period, mtDNA copy number was significantly decreased compared with the WT mice (Fig. 11*A*). Similar results were obtained when adult R26-hTP-KI mice without TPI treatment were examined, although mtDNA in the quadriceps was decreased more than 98%, which was more severe than the 78% decrease in juvenile R26-hTP-KI mice (Fig. 11*B*). The decrease in mtDNA copy number in R26-hTP-KI mice was partially recovered by TPI treatment; for example, in quadriceps, there was a 96% to 61% decrease compared with WT mice (Fig. 11*C*). A similar recovery was also observed in other tissues (data not shown).These results suggested that depletion of plasma thymidine caused decreases in mtDNA level, which resulted in mitochondrial myopathy in R26-hTP-KI mice.

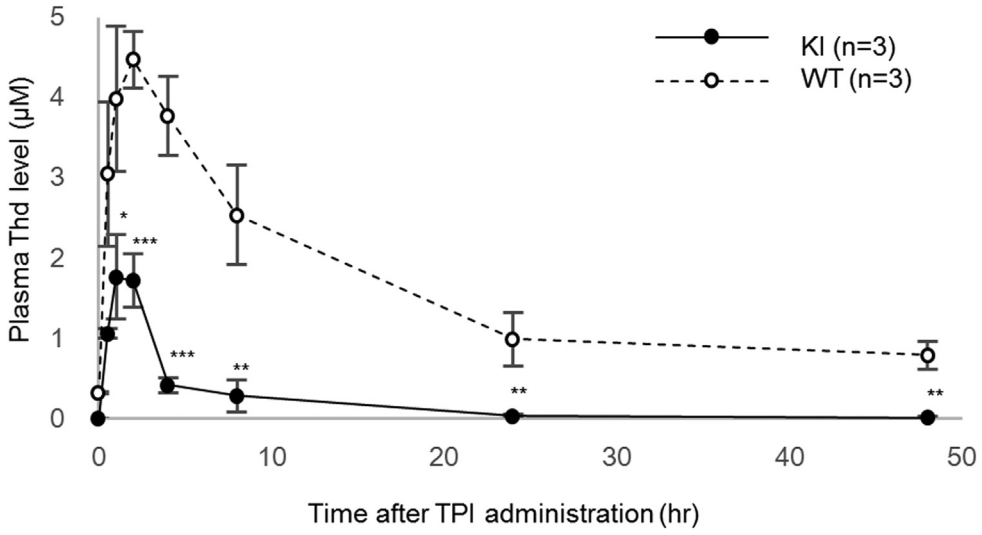

Figure 7. Time course of plasma thymidine level after TPI administration. Plasma thymidine levels in WT (*open circles*, n = 3) and KI (*closed circles*, n = 3) mice at indicated time points after the TPI treatment. Data are shown as means ± SD. *$p < 0.05$, **$p < 0.01$ and ***$p < 0.001$ compared with the WT mice. TPI, thymidine phosphorylase inhibitor.

Table 1
Plasma nucleoside levels after TPI administration

	Plasma nucleoside level (μM)					
	Thymidine		Uridine		Cytidine	
Time (h)	WT	KI	WT	KI	WT	KI
0	0.32 ± 0.02	<0.01	1.67 ± 0.36	1.91 ± 1.03	0.55 ± 0.11	0.62 ± 0.15
0.5	3.05 ± 0.90	1.06 ± 0.06*	2.24 ± 1.65	1.17 ± 0.18	0.69 ± 0.23	0.61 ± 0.04
1	3.98 ± 0.90	1.76 ± 0.52*	2.47 ± 0.70	1.80 ± 0.36	1.00 ± 0.12	0.96 ± 0.24
2	4.47 ± 0.36	1.72 ± 0.34***	1.96 ± 0.41	1.62 ± 0.77	1.03 ± 0.23	1.04 ± 0.31
4	3.77 ± 0.49	0.41 ± 0.09***	2.46 ± 0.51	1.53 ± 0.59	1.67 ± 0.12	1.13 ± 0.47
8	2.53 ± 0.62	0.28 ± 0.20**	3.14 ± 0.75	1.60 ± 0.68	2.04 ± 0.50	1.44 ± 0.46
24	0.99 ± 0.34	0.03 ± 0.02**	2.05 ± 0.77	1.53 ± 0.94	0.87 ± 0.35	0.77 ± 0.22
48	0.79 ± 0.17	0.01 ± 0.01**	2.87 ± 1.64	1.33 ± 0.33	1.05 ± 0.40	0.87 ± 0.21

	Plasma nucleoside level (μM)			
	Adenosine		Guanosine	
Time (h)	WT	KI	WT	KI
0	<5 nM	<5 nM	<12.5 nM	<12.5 nM
0.5	<5 nM	<5 nM	<12.5 nM	<12.5 nM
1	<5 nM	<5 nM	<12.5 nM	<12.5 nM
2	<5 nM	<5 nM	<12.5 nM	<12.5 nM
4	<5 nM	<5 nM	<12.5 nM	<12.5 nM
8	<5 nM	<5 nM	<12.5 nM	<12.5 nM
24	<5 nM	<5 nM	<12.5 nM	<12.5 nM
48	<5 nM	<5 nM	<12.5 nM	<12.5 nM

Plasma nucleoside level in WT (n = 3) and KI (n = 3) mice at indicated time points after TPI treatment. Data are shown as means ± SD. $^{*}p < 0.05$, $^{**}p < 0.01$ and $^{***}p < 0.001$ compared with the WT mice.
Abbreviation: TPI, thymidine phosphorylase inhibitor.

Discussion

It remains an unsolved question why plasma thymidine levels are higher in mice than other mammals including humans (8, 20), and the impact of reducing plasma thymidine to undetectable levels in mice, as in humans, is unknown. It was reported that the administration of a polyethylene glycol conjugate of TP (PEG-TPase) decreased plasma thymidine levels from 0.7–1.5 μM to <0.03 μM in mice (21, 22); however,

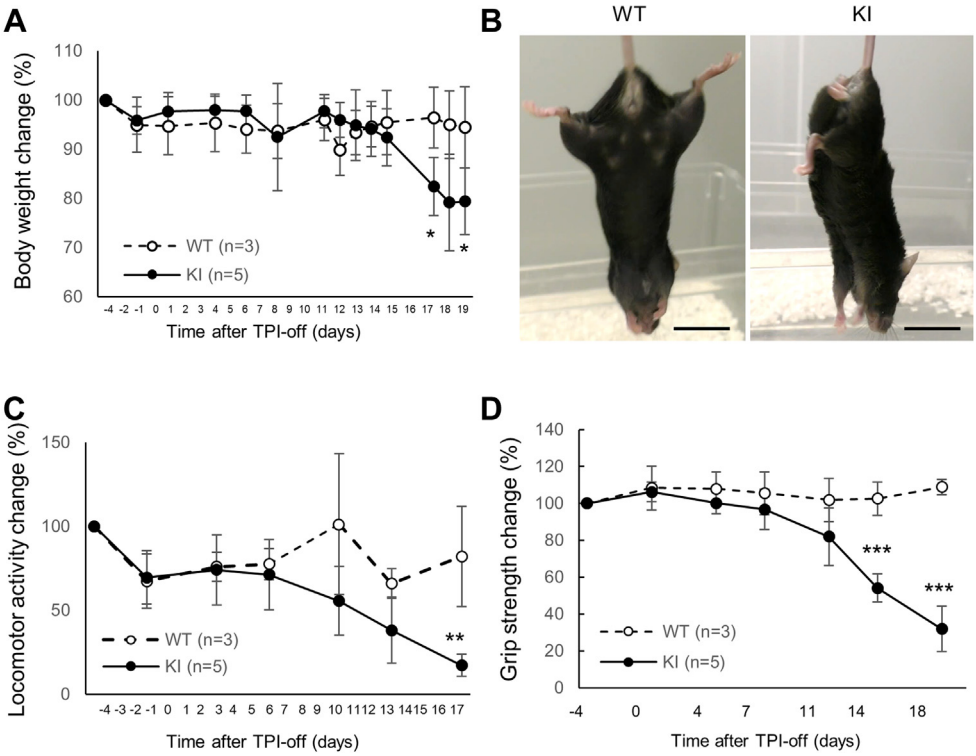

Figure 8. Hind-limb paralysis in R26-hTP-KI mice. *A*, bodyweight change of WT (*open circles*, n = 3) and KI (*closed circles*, n = 5) mice after the last TPI treatment (day −4). Results are shown as means ± SD percentages to the bodyweight at day −4. $^{*}p < 0.05$ compared with the WT mice. *B*, photograph of WT (*left*) and KI (*right*) mice hanging by the tail on day 17. The scale bar represents 2 cm. *C*, locomotor activity and *D*, grip strength of WT (*open circles*, n = 3) and KI (*closed circles*, n = 5) mice after the last TPI treatment (day −4). Results are shown as means ± SD percentages to the value at day −4. $^{**}p < 0.01$ and $^{***}p < 0.001$ compared with the WT mice. TPI, thymidine phosphorylase inhibitor.

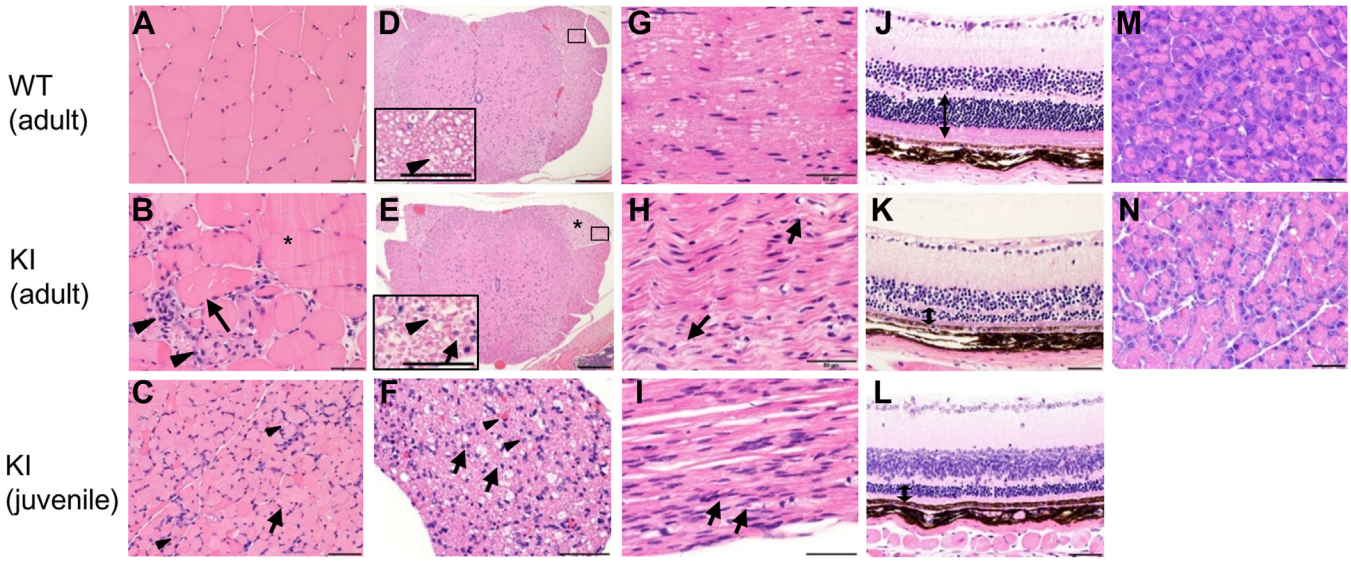

Figure 9. Histological analysis of tissues from R26-hTP-KI mice. *A*, representative H&E staining of WT and KI tissues. *A–C*, WT (adult) and KI (adult and juvenile) quadriceps. The necrotic muscle fibers infiltrated by macrophages are indicated by *arrowheads*. Degenerated muscle fibers with hyalinized muscle cells are indicated by an *arrow*. Nonuniformly striped pattern is shown by an *asterisk*. *D–F*, WT (adult) and KI (adult and juvenile) spinal cord. As indicated by an *asterisk*, the ventral root of the spinal nerve in KI mice shows a pale appearance compared with that in WT mice. Normal axon and myelin sheath structure are shown by an *arrowhead* in *D*. Atrophic axons and myelin sheaths are indicated by *arrowheads* in *E* and *F*. Increased reactive cells are shown by *arrows*. *G–I*, WT (adult) and KI (adult and juvenile) sciatic nerve. Digestion chambers are indicated by *arrows*. *J–L*, WT (adult) and KI (adult and juvenile) retina. *Bidirectional arrows* indicate outer nuclear layer, and rod and cone layer. *M* and *N*, WT (adult) and KI (adult) pancreas. Eosinophilic region was increased, whereas the basophilic region was decreased. The scale bars represent (*A*, *B*, *F–K*, *M*, and *N*), 50 μm; (*D* and *E*), 200 μm; and inserts, 50 μm; (*C* and *L*), 100 μm.

study of the long-term effects of plasma thymidine depletion in mice was challenging due to difficulties in the continuous administration of PEG-TPase. To our knowledge, therefore, this is the first report to describe that the systemic expression of human TP in mice dramatically reduced plasma thymidine levels and resulted in growth retardation accompanied by neurodegeneration and muscular atrophy. It is unlikely that these pathological phenotypes of R26-hTP-KI mice were caused by unknown genetic mutation(s) introduced during the establishment of the transgenic animals, since they were completely rescued by administration of TPI (Fig. 5*A*), noting that TPI does not inhibit thymidine kinase, uridine phosphorylase, orotate phosphoribosyltransferase, or dihydropyrimidine dehydrogenase, which metabolize pyrimidine and their nucleotides (6). In humans, high TP activity is observed in highly vascularized tissues such as liver, small intestine, kidney, and placenta, which may contribute to the systemic clearance of thymidine (23). In addition, levels of TP activity in the human small intestine, liver, and kidney were reported as 1121, 1817, and 234 nmol/h/mg, respectively (24), values that

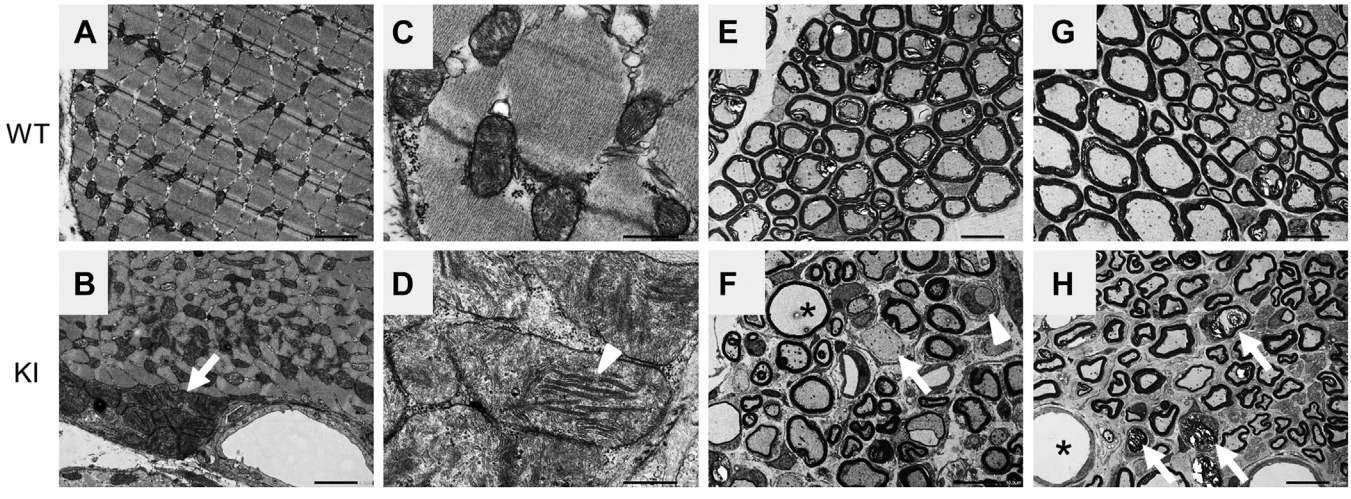

Figure 10. Electron microscopy of tissues from R26-hTP-KI mice. Electron microscope images of WT and KI tissues. *A–D*, WT and KI quadriceps. The *arrow* indicates an accumulation of mitochondria beneath the fascia. The *arrowhead* shows giant mitochondria containing linearized cristae. *E* and *F*, WT and KI spinal cord. The *arrow* and *arrowhead* indicate a demyelinated axon and a Schwann cell repairing the myelin sheath, respectively. The *asterisk* shows a vacuole-like structure surrounded by myelin sheath, containing no axon but low electron density material. *G* and *H*, WT and KI sciatic nerve. *Arrows* indicate degenerated axons. The *asterisk* shows a vacuole-like structure surrounded by myelin sheath. The scale bars represent (*A* and *B*), 2 μm; (*C* and *D*), 500 nm; (*E–H*), 10 μm.

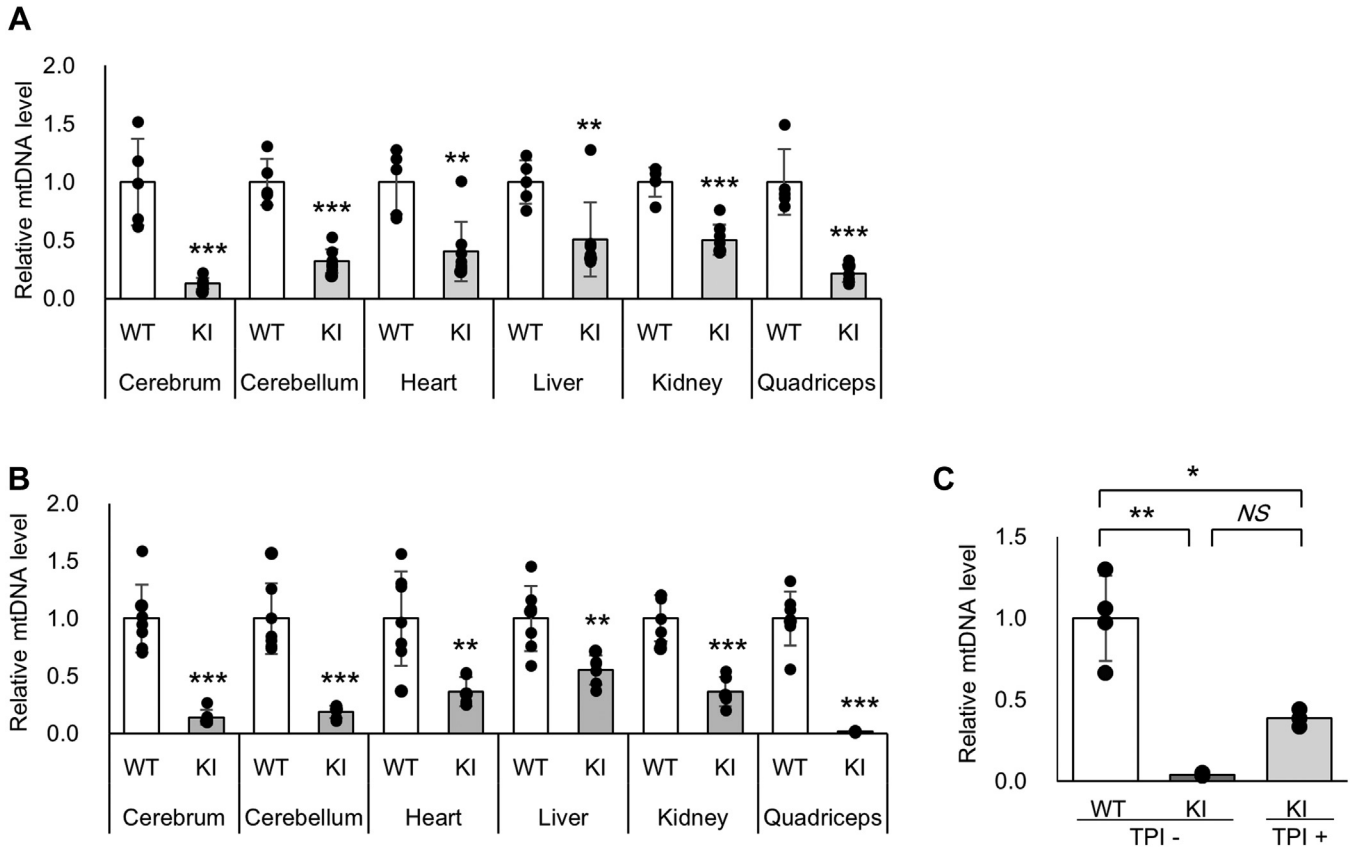

Figure 11. Depletion of mitochondrial DNA in R26-hTP-KI mice. *A*, quantification of mtDNA level in the cerebrum, cerebellum, heart, liver, kidney, and quadriceps of juvenile WT (n = 5) and KI (n = 8) mice and *B*, adult WT (n = 7) and KI (n = 6) mice. *C*, quantification of mtDNA level in the quadriceps of WT (n = 4) and KI mice with or without TPI treatment (n = 3). Results are shown relative to the WT mice (means ± SD). *$p < 0.05$,**$p < 0.01$, ***$p < 0.001$.

were closer to those in R26-hTP-KI mice compared with WT mice (Fig. 4*B*). These results suggested that systemically elevated TP activity in the R26-hTP-KI mice directly caused the decrease in plasma thymine level. Plasma thymidine level was not changed when the human TP gene was knocked into the mouse *Upp1* locus, which shows a broader expression pattern than the *Tymp* locus (Fig. 2*C*). Therefore, not only a broad tissue expression pattern but also a high expression profile under the CMV promoter inserted into the *Gtrosa26* locus seems important to reduce plasma thymidine levels in mice. Differences in substrate specificity and enzymatic kinetics between human and mouse TP (7) may contribute to the decrease in plasma thymidine levels. At the same time, TP activity in human heart and muscle was lower (40 and 55 nmol/h/mg, respectively) than in other tissues (24), while TP was highly expressed in the heart of R26-hTP-KI mice (Fig. 4). Since TP itself and the degradation products of thymidine and thymine (2-deoxy-D-ribose and beta-amino-iso-butyric acid, respectively) had chemotactic and angiogenic activities (2, 25, 26, 27), we could not rule out the possibility that high TP activity in muscle cells, rather than plasma thymidine depletion, directly caused muscular atrophy in R26-hTP-KI mice; however, this seemed unlikely, since thymidine administration partially rescued the lethal phenotype of R26-hTP-KI mice (Fig. 5*B*).

Another remarkable feature of the R26-hTP-KI model is that the overexpressed TP activity can be regulated by TPI administration, which enabled us to rescue the lethal phenotype of R26-hTP-KI mice and explore the effect of plasma thymidine depletion in adult mice, which resulted in hind-limb paralysis with similar pathological features observed around the weaning period. Notably, plasma thymidine levels in R26-hTP-KI mice were rapidly increased, reached a maximum level 2 h after TPI administration, and then were promptly restored to undetectable levels within 24 h (Fig. 7). Similar changes in plasma thymidine levels were observed in the WT mice treated with TPI, which was consistent with the previous report (6). Nevertheless, at least a twice-weekly administration is sufficient to rescue the lethal phenotype of R26-hTP-KI mice. In addition, it took approximately 2 weeks for the R26-hTP-KI mice to show the onset of the pathological phenotype after the last TPI administration. These results suggested that not a constant but a transient (<24 h) elevation of plasma thymidine levels is sufficient to maintain normal functions of neuronal and muscle cells. Since the bodyweight of the R26-hTP-KI mice was slightly lower than that of the WT mice after long-term administration of TPI (Fig. 6), we cannot rule out the possibility that transient elevation of plasma thymidine levels may not fully rescue the phenotype of R26-hTP-KI mice. This possibility may be supported by the fact that the mtDNA copy

number in R26-hTP-KI mice treated with TPI was still lower than that in WT mice (Fig. 11*C*).

It remains unclear why depletion of plasma thymidine caused neuronal degeneration and muscle atrophy in R26-hTP-KI mice. Since abnormal morphology of mitochondria was observed in the skeletal muscle and spinal cord (Fig. 10), and mtDNA was decreased in various tissues (Fig. 11), it seems likely that a failure in mitochondrial function should be involved in the pathological phenotype of R26-hTP-KI mice. It was reported that Tk2 KO mice showed growth retardation and mtDNA depletion in multiple tissues (14, 15), as observed in R26-hTP-KI mice. Tk2 is expressed in mitochondria and converts thymidine to thymidine monophosphate (dTMP) to maintain the mitochondrial deoxyribonucleotide pool, while Tk1, an isozyme of Tk2, is expressed in the cytosol (3). Mitochondrial thymidine is supplied from the cytosol and is converted to dTMP by Tk2, or dTMP synthesized in the cytosol by Tk1 is imported into the mitochondria (28, 29). Therefore, it might be possible that the human TP highly expressed in the cytosol consumes both the cytosolic and mitochondrial thymidine pools, which results in the depletion of the mitochondrial dTMP pool, although the pool of mitochondrial dNTPs is assumed to be distinct from the cytoplasmic pool in the physiological state (30). Given that the mitochondrial dNTP pool is depleted in R26-hTP-KI mice, it is conceivable that the mtDNA level is decreased through inhibition of its synthesis. This hypothesis is consistent with the fact that Tk2 KO mice died earlier (2–3 weeks of age) than R26-hTP-KI mice (3–4 weeks of age, where Tk2 activity should be present), while Tk1 KO mice died by 6 to 10 months (31), which is much longer than Tk2 KO or R26-hTP-KI mice. No histological abnormalities were observed in the brain, heart, liver, and kidney of R26-hTP-KI mice (data not shown), while more than a 50% decrease in the mtDNA level was observed in these tissues. Since the mtDNA level was most severely decreased in the quadriceps of R26-hTP-KI mice showing hind-limb paralysis (Fig. 11*B*), R26-hTP-KI mice may develop symptoms when the mtDNA level reaches a threshold level, as observed in human patients, which is generally when more than 80 to 90% of total mitochondria are affected (32). This hypothesis is consistent with the result that the TPI-treated R26-hTP-KI mice did not show hind-limb paralysis, while the mtDNA level in the quadriceps was ∼40% of that of WT mice (Fig. 11*C*).

It also remains uncertain how decreases in mtDNA copy number affect mitochondrial function, since we could not detect a clear reduction in the protein expression level and enzymatic activity of MT-CO1, which is encoded by mtDNA, while MT-CO1 has been reported to be decreased in Tk2 mutant mice showing a similar phenotype to our model (15, 16). Nevertheless, since abnormal morphology of mitochondria was clearly shown by electron microscopy in the quadriceps of R26-hTP-KI mice (Fig. 10, *B* and *D*), it seems likely that mitochondrial function might be affected. Further analyses of mitochondrial function are required in future studies.

In humans, loss of TK activity by homozygous mutation in the TP gene increases plasma thymidine levels and the development of MNGIE with mtDNA depletion takes a long time (4). In order to establish a mouse model for MNGIE, Tymp/Upp1-doubly KO (TP/UP-DKO) mice were generated because thymidine is catalyzed by both TP and UP in mice. However, the TP/UP-DKO mice showed neither peripheral neuropathy nor myopathy, while histological abnormality and mtDNA depletion were observed only in the brain (10, 11). In contrast, the R26-hTP mice showed decreased plasma thymidine levels in an opposite manner to human MNGIE, which resulted in an abnormal phenotype in the spinal cord and skeletal muscle, as well as mtDNA depletion in multiple tissues. Therefore, the model mice appear to recapitulate some of the clinical features of MNGIE better than the previously reported TP/UP-DKO model. Imbalance of the mitochondrial deoxyribonucleotide pool leads to the accumulation of mutations in mtDNA and its depletion (33). Since plasma thymidine levels are higher in mice (about 1–2 μM) than in humans, the mitochondrial deoxyribonucleotide pool balance is more likely to be affected by the depletion of plasma thymidine in R26-hTP-KI mice than by the increase of plasma thymidine in TP/UP-DKO mice. It is also of interest that pigmentary retinal degeneration (34) and abnormality in exocrine pancreas (35), part of the symptoms of mitochondrial depletion syndrome including MNGIE, were observed in R26-hTP-KI mice. It has been reported that there are some differences in purine/pyrimidine metabolism between rodents and humans. For example, in humans, the activities of hypoxanthine phosphoribosyl transferase and cytidine deaminase were higher (36, 37), whereas that of xanthine oxidoreductase was lower (38) compared with rodents. Therefore, our present results demonstrate the importance of understanding species differences when generating animal model.

In summary, we successfully established R26-hTP-KI mice that express human TP systemically and showed undetectable plasma thymidine levels as observed in humans. In addition, plasma thymidine levels could be controlled by TPI administration and continuous depletion of plasma thymidine caused a decrease in mtDNA levels, which resulted in the onset of symptoms similar to human mitochondrial depletion syndrome such as neurodegeneration, muscle atrophy, and neuro-ophthalmic and exocrine pancreatic abnormalities. These results indicate that our R26-hTP-KI mouse model should provide a new animal model for mitochondrial diseases, and clarification of the differences in nucleotide metabolism between humans and mice will assist in better understanding of mitochondrial depletion syndrome.

Experimental procedures

Construction of targeting vectors

A targeting vector for the mouse Rosa26 locus was constructed as described (39). A 1.1-kbp DNA fragment for the short homology arm (SHA) was PCR amplified using 35 cycles of 98 °C for 30 s and 68 °C for 1 min. The following primers were used: R26-SHA-F1 (5′-GTCGACAGGCCCTCCGAGCGTGGTGGA-3′) and R26-SHA-R1 (5′-AGATCTCGAGTCTAGAAAGACTGGAGTTGCAGAT-3′). Similarly, a 4.3-kbp

DNA fragment for the long homology arm (LHA) was PCR amplified using 35 cycles of 98 °C for 30 s and 68 °C for 5 min. The following primers were used: R26-LHA-F1 (5′-ATTTAAATCTAGAAGATGGGCGGGAGTCTTCTGGG-3′) and R26-LHA-R1 (5′-ATTTAAATGCGATCGCTTAATTAAGCTAGATGTCCTGAAATATTTCTATC-3′). The SHA and LHA fragments, floxed PGK-Neo-bpA and PGK-DT-a cassettes were subcloned into pBluescript to construct the pRosa26-lox-neo plasmid. A human TP cDNA (GenBank accession number: NM_001113755) was purchased from Thermo Fisher Scientific and cloned into the pLVSIN-CMV Neo plasmid (Takara Bio). The resulting pLVSIN-CMV-hTP plasmid was digested with Cla I and Not I to prepare a 2.1-kbp CMV-hTP cassette, which was inserted into the Cla I site of the pRosa26-lox-neo plasmid.

Generation of transgenic animals

An ES cell line (CMTI-1) was purchased from Millipore. ES cells (2×10^7 cells) were electroporated with 50 μg of the linearized targeting vector, and G418-resistant clones were screened by PCR (35 cycles of 94 °C for 30 s, 60 °C for 1 min, and 72 °C for 2 min) using the following primers: R26-EF1-F1 (5′-CTCAGAGAGCCTCGGCTAGGTAGGGGATCG-3′) and R26-screen-Rv (5′-CGATAAGCTTGATAGATCTCGAGTCTAGAA-3′). Homologous recombinant clones with a 1.2-kbp PCR product were confirmed by Southern blot analysis and were then injected into C57BL/6N blastocysts. Germ line–transmitted chimeras were crossbred with C57BL/6N females (Charles River) to obtain heterozygous offspring (*Gtrosa26*$^{tm3(CMV\text{-}TYMP)Tai}$). Both WT and KI alleles were identified by PCR (35 cycles of 98 °C for 30 s, 60 °C for 1 min, and 72 °C for 1 min) with the following primers: R26-common-F1 (5′-CTCGTGTTCGTGCAAGTTGAGT-3′), R26-WT-R1 (5′-ATGACTACCTATCCTCCCATTT-3′), and R26-KI-R1 (5′-CGATAAGCTTGATAGATCTCGAGT-3′). All mice were maintained under standard animal housing conditions (light phase, 8:00 AM–8:00 PM; dark phase, 8:00 PM–8:00 AM) and were ad libitum fed a regular chow diet, CE-2 (CLEA). R26-hTP-KI mice were maintained with or without intraperitoneal administration (*i.p.*) of 50 mg/ml/Kg of TPI (Taiho Pharmaceuticals). All animal procedures were conducted in compliance with the National Institutes of Health (NIH) guidelines and were approved by the Taiho Institutional Animal Care and Use Committee.

Quantitative RT-PCR analysis

Total RNA was prepared from mouse livers using Isogen (Wako Pure Chemical Industries) and RNeasy (QIAGEN). DNase I–treated total RNA (3 μg) was used to synthesize cDNA with SuperScript III First-Strand Synthesis SuperMix (Thermo Fisher Scientific). Real-time RT-PCR contained, in a final volume of 50 μl, 0.75 μg of cDNA, 2.5 μl of 20x TaqMan Assay Mix for human *TYMP* (Assay ID: Hs00157317_m1) or mouse *Tymp* (Assay ID: Mm01301807_g1), 2.5 μl of 20x TaqMan Assay Mix for ribosomal RNA (4319413E), and 25 μl of 2x TaqMan UMM (all from Thermo Fisher Scientific). The reaction was performed in a 96-well optical reaction plate using the PRISM 7900HT Sequence Detection System (Thermo Fisher Scientific). Expression data were normalized to the ribosomal RNA expression level.

Western blotting analysis

Tissues were prepared from 4-week-old heterozygous KI and litter-control WT mice and homogenized by sonication in lysis buffer (50 mM Tris-HCl [pH 7.2], 1% Triton X-100, 0.02% 2-mercaptoethanol) containing proteinase inhibitor cocktail (Sigma-Aldrich). Lysates were centrifuged at 20,000*g* for 30 min at 4 °C, and 50 to 100 μg of the supernatant was subjected to SDS-PAGE, transferred to membranes, and immunoblotted with anti-human TP (1: 200, IBL) or GAPDH (1:1000, Cell Signaling Technology) antibody. Blotting images were analyzed using an Amersham Imager 600 with ImageQuant TL (Fujifilm).

Determination of TP activity

TP activity was measured according to the spectrophotometric method described previously (40) with slight modifications. Briefly, 50 to 100 μg of the supernatant protein was incubated with 10 mM thymidine in reaction buffer (100 mM potassium phosphate buffer, pH 7.4) in a total volume of 20 μl. After incubation for 5 to 6 h at 37 °C, the reaction was terminated by the addition of 180 μl of 0.3 N NaOH. Absorbance at 300 nm was measured using a SpectraMax Plus 384 microplate reader (Molecular Devices). The amount of thymine formed was determined using a standard plot (0, 0.5, 1, 2, and 5 mM). Since thymidine phosphorolysis in murine tissue may also be catalyzed by UP (41), thymidine degradation activity in the presence of 1 mM TPI was measured and subtracted from the total activity, with negative values treated as zero. Enzyme activity was expressed as nanomoles of thymine formed per hour and milligram of protein.

Measurement of plasma thymidine level with mass spectrometry

Twenty microliters of the plasma sample was mixed with 20 μl of methanol. After adding 20 μl of 4 μM trifluorothymidine (Sigma-Aldrich) as an internal standard and 300 μl of acetonitrile, samples were centrifuged at 3000*g* for 10 min at 4 °C. Three hundred microliters of the supernatant was dried at 40 °C using a Turbo Vap 96 (Biotage), resolved in 100 μl of water, and injected into a Prominence UFLC HPLC apparatus (SHIMADZU CORPORATION) with an L-column2 ODS reverse phase column (Chemicals Evaluation and Research Institute) and analyzed with the API 4000 LC-MS/MS System (AB SCIEX). Quantitation of thymidine was carried out using Analysis 1.5.1 software (AB SCIEX) based on external standards.

Histological analysis

Tissue samples were fixed in neutral-buffered formalin, except for the eyes, which were fixed in Davidson fixative, and then embedded in paraffin. The sample sections (2 μm) were prepared and stained with H&E. For electron microscopy,

samples were fixed in 4% paraformaldehyde, then 1% osmium tetroxide, and dehydrated in graded ethanol, followed by embedding in epoxy resin (TAAB Laboratories Equipment Ltd). Sample sections (80 nm) were prepared, stained by uranyl acetate and lead staining solution, and examined under an electron microscope, JEM-1400 (JEOL Ltd).

Locomotor activity

Spontaneous locomotor activity was continuously recorded in 1-min bins for 22 h using on-cage infrared movement detectors linked to a monitoring system (Melquest). After the last administration of TPI (day −4) and measurement of bodyweight, R26-hTP-KI (n = 5, two males and three females) and WT mice (n = 3, one male and two females) were housed in individual new cages with free access to food and water. Bodyweight and locomotor activity were measured on day 0, 3, 6, 10, 13, and 17. Data are shown in terms of percent relative to those at last TPI administration (day −4).

Grip strength

Grip strength was measured using a GPM-100B grip strength meter (Melquest) after measuring locomotor activity. Mice holding on to a metal grid with four limbs were pulled backward by the tail. The grip strength of each mouse was measured five times and the average value was used as the individual value for each mouse. Data are shown in terms of percent relative to those at last TPI administration (day −4).

MtDNA copy number

Total DNAs were purified by a standard phenol/chloroform extraction procedure from the cerebrum, cerebellum, heart, liver, kidney, and quadriceps of R26-hTP-KI mice (n = 8 and n = 6 for juveniles and adults, respectively) and WT mice (n = 5 and n = 7 for juveniles and adults, respectively), then lysed with Proteinase K (Thermo Fisher Scientific). Mouse mtDNA was quantitated by real-time PCR using the ABI PRISM 7900HT sequence detection system (Thermo Fisher Scientific) as described (42) using primers and probes for the murine mtDNA encoded gene Mt-co1 (mitochondrially encoded cytochrome c oxidase I) and the single-copy nuclear gene Ndufv1 (NADH:ubiquinone oxidoreductase core subunit V1), respectively. Sequences of each primer and probe are shown below.

Mt-co1 Fw primer: 5′-TGC TAG CCG CAG GCA TTA C-3′;

Mt-co1 Rv primer: 5′-GGG TGC CCA AAG AAT CAG AAC-3′;

Mt-co1 probe: FAM-AAC CTA AAC ACA ACT TTC TTT GAT CCC GCT GG-DB;

Ndufv1 Fw primer: 5′-CTT CCC CAC TGG CCT CAA G-3′;

Ndufv1 Rv primer: 5′-CCA AAA CCC AGT GAT CCA GC-3′;

Ndufv1 probe: YAK-AGC CCT CAG ATG GCA GGT TTG G-DB.

The ratios of Mt-co1/Ndufv1 quantities were calculated, and the data are expressed in terms of percent relative to WT mice.

Statistical analysis

All data are shown as means ± standard deviation. Statistical differences between two groups were examined using Student's *t* test. For multiple comparisons, statistical analysis was performed using a repeated measures ANOVA and differences among each group were analyzed using the Tukey–Kramer test.

Data availability

All data are contained within the article.

Acknowledgments—We are grateful to Hidenori Fujita, Fumitaka Harada, Megumu Okada, Kenjiro Ito, Masaki Yamada, Shingo Tsuji, Sakiho Tanaka, and Toshihiro Osada for checking the data. We also thank Masanori Sagae and Kazuki Sakamoto for technical advice on measuring plasma nucleoside concentration.

Author contributions—N. H., Kenichi Matsuo, and Kazutaka Miyadera conceptualization; N. H., H. N., H. Y., Kenji Matsubara, T. S., and A. G. methodology; N. H., H. N., H. Y., Kenji Matsubara, and T. S. investigation; N. H. writing – original draft; N. H., T. Y., Kenichi Matsuo, and Kazutaka Miyadera writing – review & editing.

Conflict of interest—The authors declare that they have no conflicts of interest with the contents of this article.

Abbreviations—The abbreviations used are: dTTP, deoxythymidine triphosphate; KI, knock-in; LHA, long homology arm; MDS, mtDNA depletion syndrome; MNGIE, mitochondrial neurogastrointestinal encephalopathy; SHA, short homology arm; TK, thymidine kinase; TP, thymidine phosphorylase; TPI, thymidine phosphorylase inhibitor; UP, uridine phosphorylase.

References

1. Mikhailopulo, I. A., and Miroshnikov, A. I. (2010) New trends in nucleoside biotechnology. *Acta Naturae* **2**, 36–59
2. Brown, N. S., and Bicknell, R. (1998) Thymidine phosphorylase, 2-deoxy-D-ribose and angiogenesis. *Biochem. J.* **334**, 1–8
3. Munch-Petersen, B. (2010) Enzymatic regulation of cytosolic thymidine kinase 1 and mitochondrial thymidine kinase 2: a mini review. *Nucleosides Nucleotides Nucleic Acids* **29**, 363–369
4. Nishino, I., Spinazzola, A., and Hirano, M. (1999) Thymidine phosphorylase gene mutations in MNGIE, a human mitochondrial disorder. *Science* **283**, 689–692
5. Nishino, I., Spinazzola, A., and Hirano, M. (2001) MNGIE: from nuclear DNA to mitochondrial DNA. *Neuromuscul. Disord.* **11**, 7–10
6. Fukushima, M., Suzuki, N., Emura, T., Yano, S., Kazuno, H., Tada, Y., *et al.* (2000) Structure and activity of specific inhibitors of thymidine phosphorylase to potentiate the function of antitumor 2'-deoxyribonucleosides. *Biochem. Pharmacol.* **59**, 1227–1236
7. el Kouni, M. H., el Kouni, M. M., and Naguib, F. N. (1993) Differences in activities and substrate specificity of human and murine pyrimidine nucleoside phosphorylases: implications for chemotherapy with 5-fluoropyrimidines. *Cancer Res.* **53**, 3687–3693
8. van der Wilt, C. L., Backus, H. H., Smid, K., Comijn, L., Veerman, G., Wouters, D., *et al.* (2001) Modulation of both endogenous folates and thymidine enhance the therapeutic efficacy of thymidylate synthase inhibitors. *Cancer Res.* **61**, 3675–3681
9. Jackman, A. L., Taylor, G. A., Calvert, A. H., and Harrap, K. R. (1984) Modulation of anti-metabolite effects. Effects of thymidine on the efficacy of the quinazoline-based thymidylate synthetase inhibitor, CB3717. *Biochem. Pharmacol.* **33**, 3269–3275

10. Haraguchi, M., Tsujimoto, H., Fukushima, M., Higuchi, I., Kuribayashi, H., Utsumi, H., *et al.* (2002) Targeted deletion of both thymidine phosphorylase and uridine phosphorylase and consequent disorders in mice. *Mol. Cell. Biol.* **22**, 5212–5221
11. Lopez, L. C., Akman, H. O., Garcia-Cazorla, A., Dorado, B., Marti, R., Nishino, I., *et al.* (2009) Unbalanced deoxynucleotide pools cause mitochondrial DNA instability in thymidine phosphorylase-deficient mice. *Hum. Mol. Genet.* **18**, 714–722
12. Cao, D., Leffert, J. J., McCabe, J., Kim, B., and Pizzorno, G. (2005) Abnormalities in uridine homeostatic regulation and pyrimidine nucleotide metabolism as a consequence of the deletion of the uridine phosphorylase gene. *J. Biol. Chem.* **280**, 21169–21175
13. Saada, A., Shaag, A., Mandel, H., Nevo, Y., Eriksson, S., and Elpeleg, O. (2001) Mutant mitochondrial thymidine kinase in mitochondrial DNA depletion myopathy. *Nat. Genet.* **29**, 342–344
14. Zhou, X., Solaroli, N., Bjerke, M., Stewart, J. B., Rozell, B., Johansson, M., *et al.* (2008) Progressive loss of mitochondrial DNA in thymidine kinase 2-deficient mice. *Hum. Mol. Genet.* **17**, 2329–2335
15. Akman, H. O., Dorado, B., Lopez, L. C., Garcia-Cazorla, A., Vila, M. R., Tanabe, L. M., *et al.* (2008) Thymidine kinase 2 (H126N) knockin mice show the essential role of balanced deoxynucleotide pools for mitochondrial DNA maintenance. *Hum. Mol. Genet.* **17**, 2433–2440
16. Bartesaghi, S., Betts-Henderson, J., Cain, K., Dinsdale, D., Zhou, X., Karlsson, A., *et al.* (2010) Loss of thymidine kinase 2 alters neuronal bioenergetics and leads to neurodegeneration. *Hum. Mol. Genet.* **19**, 1669–1677
17. Zambrowicz, B. P., Imamoto, A., Fiering, S., Herzenberg, L. A., Kerr, W. G., and Soriano, P. (1997) Disruption of overlapping transcripts in the ROSA beta geo 26 gene trap strain leads to widespread expression of beta-galactosidase in mouse embryos and hematopoietic cells. *Proc. Natl. Acad. Sci. U. S. A.* **94**, 3789–3794
18. Vincent, A. E., Ng, Y. S., White, K., Davey, T., Mannella, C., Falkous, G., *et al.* (2016) The spectrum of mitochondrial ultrastructural defects in mitochondrial myopathy. *Sci. Rep.* **6**, 30610
19. Filograna, R., Mennuni, M., Alsina, D., and Larsson, N. G. (2021) Mitochondrial DNA copy number in human disease: the more the better? *FEBS Lett.* **595**, 976–1002
20. Taylor, G. A., Jackman, A. L., Calvert, A. H., and Harrap, K. R. (1984) Plasma nucleoside and base levels following treatment with the new thymidylate synthetase inhibitor CB 3717. *Adv. Exp. Med. Biol.* **165**, 379–382
21. Smith, G. K., Amyx, H., Boytos, C. M., Duch, D. S., Ferone, R., and Wilson, H. R. (1995) Enhanced antitumor activity for the thymidylate synthase inhibitor 1843U89 through decreased host toxicity with oral folic acid. *Cancer Res.* **55**, 6117–6125
22. Koszalka, G. W., Lobe, D., Stonefield, M. W., Vanhooke, J., Ferone, R., and Ellis, K. W. (1993) In vivo potentiation of acyclovir by methoxypolyethyleneglycol-thymidine phosphorylase. *Antiviral Res* **20**, 143
23. Yoshimura, A., Kuwazuru, Y., Furukawa, T., Yoshida, H., Yamada, K., and Akiyama, S. (1990) Purification and tissue distribution of human thymidine phosphorylase; high expression in lymphocytes, reticulocytes and tumors. *Biochim. Biophys. Acta* **1034**, 107–113
24. Valentino, M. L., Marti, R., Tadesse, S., Lopez, L. C., Manes, J. L., Lyzak, J., *et al.* (2007) Thymidine and deoxyuridine accumulate in tissues of patients with mitochondrial neurogastrointestinal encephalomyopathy (MNGIE). *FEBS Lett.* **581**, 3410–3414
25. Stevenson, D. P., Milligan, S. R., and Collins, W. P. (1998) Effects of platelet-derived endothelial cell growth factor/thymidine phosphorylase, substrate, and products in a three-dimensional model of angiogenesis. *Am. J. Pathol.* **152**, 1641–1646
26. Ishikawa, F., Miyazono, K., Hellman, U., Drexler, H., Wernstedt, C., Hagiwara, K., *et al.* (1989) Identification of angiogenic activity and the cloning and expression of platelet-derived endothelial cell growth factor. *Nature* **338**, 557–562
27. Miyadera, K., Sumizawa, T., Haraguchi, M., Yoshida, H., Konstanty, W., Yamada, Y., *et al.* (1995) Role of thymidine phosphorylase activity in the angiogenic effect of platelet derived endothelial cell growth factor/thymidine phosphorylase. *Cancer Res.* **55**, 1687–1690
28. Pontarin, G., Gallinaro, L., Ferraro, P., Reichard, P., and Bianchi, V. (2003) Origins of mitochondrial thymidine triphosphate: dynamic relations to cytosolic pools. *Proc. Natl. Acad. Sci. U. S. A.* **100**, 12159–12164
29. Rampazzo, C., Fabris, S., Franzolin, E., Crovatto, K., Frangini, M., and Bianchi, V. (2007) Mitochondrial thymidine kinase and the enzymatic network regulating thymidine triphosphate pools in cultured human cells. *J. Biol. Chem.* **282**, 34758–34769
30. Moraes, C. T. (2001) What regulates mitochondrial DNA copy number in animal cells? *Trends Genet.* **17**, 199–205
31. Dobrovolsky, V. N., Bucci, T., Heflich, R. H., Desjardins, J., and Richardson, F. C. (2003) Mice deficient for cytosolic thymidine kinase gene develop fatal kidney disease. *Mol. Genet. Metab.* **78**, 1–10
32. Mazat, J. P., Rossignol, R., Malgat, M., Rocher, C., Faustin, B., and Letellier, T. (2001) What do mitochondrial diseases teach us about normal mitochondrial functions...that we already knew: threshold expression of mitochondrial defects. *Biochim. Biophys. Acta* **1504**, 20–30
33. Pacitti, D., Levene, M., Garone, C., Nirmalananthan, N., and Bax, B. E. (2018) Mitochondrial neurogastrointestinal encephalomyopathy: into the fourth decade, what we have learned so far. *Front. Genet.* **9**, 669
34. Barboni, P., Savini, G., Plazzi, G., Bellan, M., Valentino, M. L., Zanini, M., *et al.* (2004) Ocular findings in mitochondrial neurogastrointestinal encephalomyopathy: a case report. *Graefes Arch. Clin. Exp. Ophthalmol.* **242**, 878–880
35. McShane, M. A., Hammans, S. R., Sweeney, M., Holt, I. J., Beattie, T. J., Brett, E. M., *et al.* (1991) Pearson syndrome and mitochondrial encephalomyopathy in a patient with a deletion of mtDNA. *Am. J. Hum. Genet.* **48**, 39–42
36. Tax, W. J., Veerkamp, J. H., Trijbels, F. J., and Schretlen, E. D. (1976) Mechanism of allopurinol-mediated inhibition and stabilization of human orotate phosphoribosyltransferase and orotidine phosphate decarboxylase. *Biochem. Pharmacol.* **25**, 2025–2032
37. Hurwitz, S. J., Otto, M. J., and Schinazi, R. F. (2005) Comparative pharmacokinetics of racivir, (+/-)-beta-2',3'-dideoxy-5-fluoro-3'-thiacytidine in rats, rabbits, dogs, monkeys and HIV-infected humans. *Antivir. Chem. Chemother.* **16**, 117–127
38. Xu, P., LaVallee, P., and Hoidal, J. R. (2000) Repressed expression of the human xanthine oxidoreductase gene. E-box and TATA-like elements restrict ground state transcriptional activity. *J. Biol. Chem.* **275**, 5918–5926
39. Soriano, P. (1999) Generalized lacZ expression with the ROSA26 cre reporter strain. *Nat. Genet.* **21**, 70–71
40. Friedkin, M., and Roberts, D. (1954) The enzymatic synthesis of nucleosides. I. Thymidine phosphorylase in mammalian tissue. *J. Biol. Chem.* **207**, 245–256
41. Krenitsky, T. A., Barclay, M., and Jacquez, J. A. (1964) Specificity of mouse uridine phosphorylase. Chromatography, purification, and properties. *J. Biol. Chem.* **239**, 805–812
42. Amthor, H., Macharia, R., Navarrete, R., Schuelke, M., Brown, S. C., Otto, A., *et al.* (2007) Lack of myostatin results in excessive muscle growth but impaired force generation. *Proc. Natl. Acad. Sci. U. S. A.* **104**, 1835–1840